

# Ac Stark shifts in a two-zone Raman interaction

P. R. Hemmer

Rome Air Development Center, Hanscom Air Force Base, Bedford, Massachusetts 01731

M. S. Shahriar, V. D. Natoli,\* and S. Ezekiel

Research Laboratory of Electronics, Massachusetts Institute of Technology, Cambridge, Massachusetts 02139

Received December 21, 1988; accepted March 27, 1989

We have measured the ac Stark effect in a two-zone stimulated Raman interaction in a sodium atomic beam. In addition, we have derived simple theoretical expressions for the ac Stark shift, based on a closed three-level system, in the  $\Lambda$  configuration, and have achieved qualitative agreement with the data. In particular, the magnitude and sense of the ac Stark shifts are found to depend on laser intensities as well as on the initial populations of the two low-lying levels of the  $\Lambda$  configuration. Specifically, the observed ac Stark shifts are smaller for larger laser intensities and also for smaller initial population differences between the two low-lying levels. The ac Stark effect must be considered for many potential applications of the Raman effect, such as a Raman clock. In this connection, we have identified conditions for the reduction of the ac Stark shift in our sodium Raman clock.

## INTRODUCTION AND BACKGROUND

Much recent work, both theoretical and experimental, has been performed to identify potential applications of the stimulated Raman interaction. These include application to the study of fundamental atom-field interactions,<sup>1-3</sup> collisional diffusion,<sup>4</sup> Raman lasers,<sup>5</sup> and new time and frequency standards.<sup>6-8</sup> For all these applications, and especially for time and frequency standards, it is important to understand thoroughly all sources of line-shape asymmetries and level shifts. The ac Stark effect is therefore of special interest because of its fundamental nature and because it produces line-shape asymmetries and level shifts that can be significant under certain conditions.

In this paper we report the results of our experimental and theoretical studies of the ac Stark effect in a two-zone stimulated Raman interaction, using a sodium atomic beam. The two-zone excitation scheme is used because it is important for potential clock applications and because it provides unique physical insights into the nature of the ac Stark effect in the stimulated Raman interaction. Previous theoretical treatments<sup>2,8</sup> of the ac Stark shifts in a Raman interaction are confined primarily to single-zone excitation and do not include the effects of saturation.

We will begin by presenting data showing the ac Stark shift in the Raman two-zone excitation scheme as a function of laser detuning for various experimental conditions, for example, different laser intensities and initial atomic state populations. This is followed by a brief derivation of simple, closed-form theoretical expressions for the Raman ac Stark shift in the two-zone excitation scheme, assuming an ideal, closed three-level system. Agreement of these simple calculations with the data is then illustrated for various cases. Next, the simple theory is augmented to account for the fact that more than three levels are involved in the interaction, and the modified theory shows improved agreement with the data. Finally, it is shown that proper choice

of experimental conditions can reduce the ac Stark shift to levels acceptable for potential clock applications.<sup>7</sup>

The stimulated Raman interaction is illustrated schematically with the three-level system in Fig. 1(a). Briefly, Raman transitions are induced between states 1 and 3 by using two laser fields, at frequencies  $\omega_1$  and  $\omega_2$ , simultaneously resonant with the intermediate state 2. Experimentally, if  $\omega_1$  is held fixed at the 1-2 transition frequency and  $\omega_2 - \omega_1$  is scanned over the 3-2 transition, a fluorescence line shape such as the one shown in Fig. 1(b) results. Here, the Raman interaction appears as a dip in fluorescence (trapped state formation<sup>1,2</sup>) that in this case occurs at the center of the  $\gamma_2$  wide 3-2 transition. Earlier studies<sup>3,4,6</sup> show that, for copropagating laser fields interacting with an atomic beam at right angles, the Raman linewidth is determined by the widths of states 1 and 3 only. State 2 greatly enhances the transition probability but does not contribute to the linewidth. Laser jitter effects are greatly reduced by generating both frequencies from the same laser with an acousto-optic frequency shifter, driven by a microwave oscillator. Thus, for long-lived states 1 and 3, the Raman linewidth becomes transit-time limited, just as for direct microwave excitation.

Ac Stark shifts in the Raman system arise when the laser fields are tuned off resonance with the intermediate state. This is illustrated in Fig. 1(c) in the case when both laser frequencies are detuned by the same amount (common-mode detuning). Such detunings produce asymmetric Raman line shapes, as shown by the data of Fig. 1(d). These asymmetries are manifestations of the ac Stark effect (light shift) in the single-zone Raman interaction.

Two-zone excitation of the stimulated Raman interaction is illustrated in Fig. 2(a). This scheme is analogous to Ramsey's method of separated-microwave-field excitation<sup>9</sup> in an atomic beam. Briefly, in separated-field excitation long-lived atomic polarizations are induced in the two interaction zones. These polarizations interfere and produce fringes

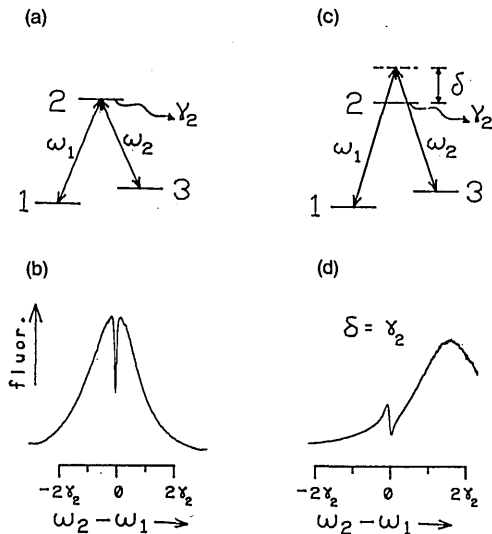


Fig. 1. (a) Schematic of stimulated resonance Raman interaction, (b) single-zone resonance Raman line shape, (c) schematic of off-resonance Raman interaction, and (d) single-zone off-resonance Raman line shape.

whose widths (measured in terms of laser difference frequency) are characteristic of the atom transit time between the two interaction zones. Figure 2(b) shows a typical Raman-Ramsey fringe line shape observed experimentally by monitoring the zone B fluorescence as the laser difference

frequency is scanned. The central fringe has a width of  $\sim 2.3$  kHz (FWHM), which is consistent with the transit time for the 15-cm interaction-zone separation and the thermal velocity of  $\sqrt{2kT/M} = 7 \times 10^4$  cm/sec for a sodium beam produced by a 400°C oven. As is well known,<sup>9</sup> the envelope function for these fringes is determined by velocity averaging, as illustrated in Fig. 2(c). The dotted curves in this figure are single-velocity fringes, which are pure cosines, and the solid curve is the velocity-averaged fringe pattern.

As will be shown below, ac Stark shifts in the two-zone Raman interaction can be expressed as a phase shift in the cosine function describing the Ramsey fringe. Such Ramsey-fringe phase shifts are well known from microwave studies and in this connection arise when the microwave excitation fields in the two excitation zones are not in phase.<sup>9</sup> These Ramsey-fringe phase shifts result in frequency shifts of the central-fringe minima and also produce line-shape asymmetries when velocity averaging is included. This is illustrated in Fig. 2(d) for the case of a constant  $\pi/2$  phase shift.

Figure 3 shows experimentally observed Raman-Ramsey fringes that are similar in appearance to the phase-shifted fringes of Fig. 2(d). All three data in Fig. 3 were obtained for a common-mode laser detuning of  $\delta = 0.8\gamma_2$  but different initial atomic state populations. Figure 3(a) corresponds to the case when all the atoms are initially placed in state 1, by optical pumping to be described below. Figure 3(b) corresponds to initially equal state 1 and 3 populations, and Fig.

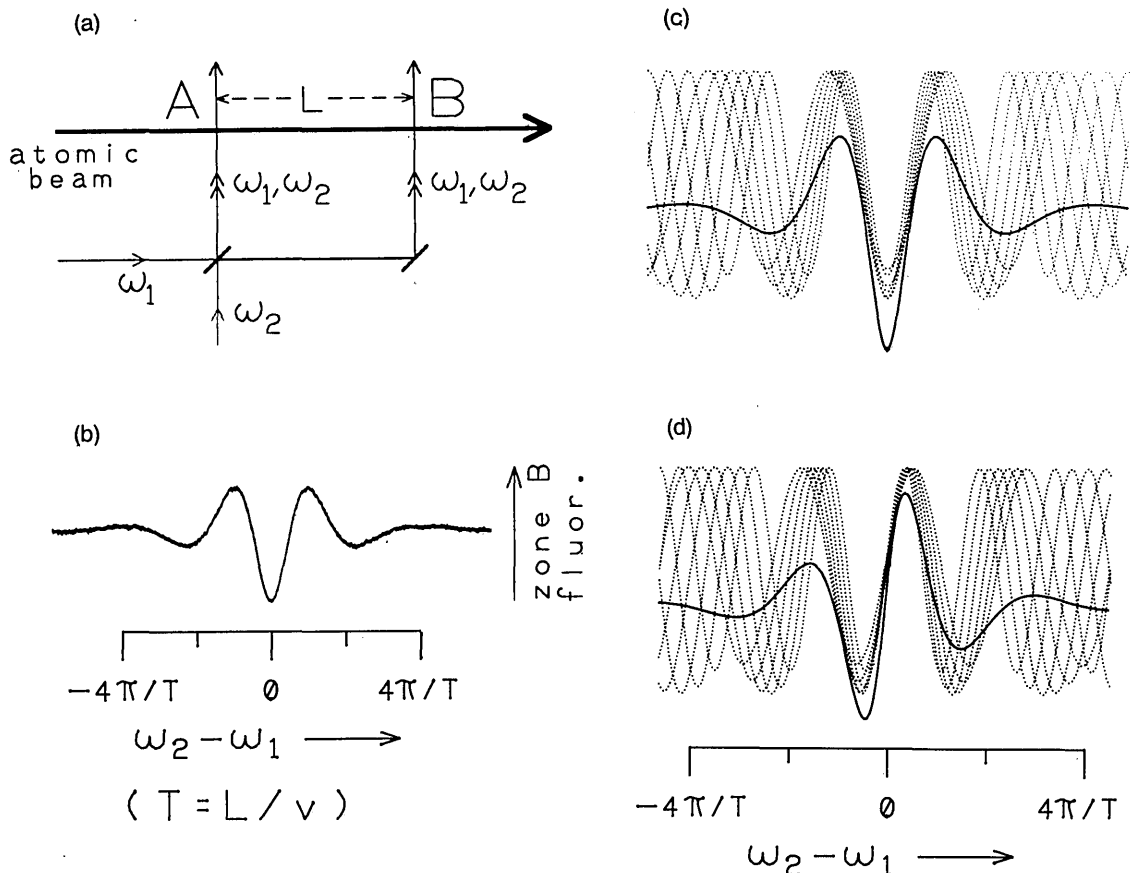


Fig. 2. (a) Schematic of separated-field Raman excitation, (b) two-zone Ramsey-fringe line shape observed in zone B fluorescence, (c) theoretical fringe shape resulting from velocity averaging, and (d) theoretical velocity-averaged fringe shape for  $\pi/2$  phase-shifted fringes.

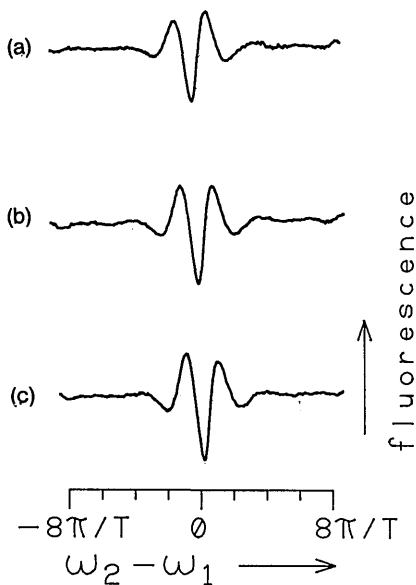


Fig. 3. Observed Ramsey-fringe asymmetries for a fixed common-mode detuning of  $\delta = 0.8\gamma_2$ . Initial populations: (a)  $\rho_{11}^0 = N, \rho_{33}^0 = 0$ ; (b)  $\rho_{11}^0 = \rho_{33}^0 = N/2$ ; (c)  $\rho_{11}^0 = 0, \rho_{33}^0 = N$ .

3(c) to all atoms initially in state 3. As can be seen, the magnitude as well as the sense of the ac-Stark-produced asymmetry depends on the initial atomic state populations. As expected, the magnitude and sense of the ac-Stark-induced asymmetry also depend on the common-mode laser detuning (not shown) for fixed initial atomic state populations. These observations will be quantified below.

## EXPERIMENT

For most applications, specifically those related to clocks, it is the frequency shift in the Ramsey-fringe central minimum, rather than the detail of the asymmetrical line shape, that is of immediate interest. Therefore in our experiment we concentrate on observing the frequency shift of the cen-

tral minimum as a function of various parameters, for example, common-mode laser detuning, initial atomic state populations, and laser intensity. Experimentally, this is accomplished by locking the laser difference frequency to the central Ramsey-fringe minimum, using a servo, and recording the stabilized difference frequency as different parameters are varied.

Figure 4 schematically illustrates the experimental setup used to measure two-zone Raman ac Stark shifts as a function of common-mode laser detuning in a sodium atomic beam. As shown, the laser field at frequency  $\omega_1$  (590 nm) is the output of a cw dye laser having 1 MHz of frequency jitter. The field at frequency  $\omega_2$  is generated from that at  $\omega_1$  by using an acousto-optic modulator, A/O(1), driven by a voltage-controlled oscillator, VCO(1). VCO(1) can be tuned over the 1–3 Raman transition frequency (1772 MHz). The laser fields at  $\omega_1$  and  $\omega_2$  are combined by using a beam splitter before exciting the atomic beam at zones A and B, as shown. Another portion of the laser beam at  $\omega_1$  is shifted by a second modulator, A/O(2) (actually a pair of modulators), so that the shifted laser frequency  $\omega_1 + \delta$  can be tuned both above and below  $\omega_1$ . This shifted laser frequency is then locked to the 1–2 transition with fluorescence produced in the reference interaction zone (REF), as shown. By using this scheme,  $\omega_1$  and  $\omega_2$  are simultaneously scanned over the 1–2 and 3–2 transitions, respectively (common mode scan), by simply tuning VCO(2). The laser in the reference zone is also used to adjust the initial state 1 and 3 populations by means of optical pumping. In this experiment, levels 1 and 3 are the  $F = 1$  and  $F = 2$  hyperfine sublevels, respectively, of the  $^2S_{1/2}$  ground state, and state 2 is the  $F = 2$  sublevel of the  $^2P_{1/2}$  state. The laser beams in zones A and B are right-circularly polarized, while the beam in the reference zone is linearly polarized. A magnetic field is applied parallel to the  $\mathbf{k}$  vectors of the laser fields. Thus only  $\sigma^+$  excitations are allowed in the interaction zones (and both  $\sigma^+$  and  $\sigma^-$  in the reference zone).

Figure 5 shows a set of data obtained with this experimental setup. Each trace is the observed two-zone ac Stark shift

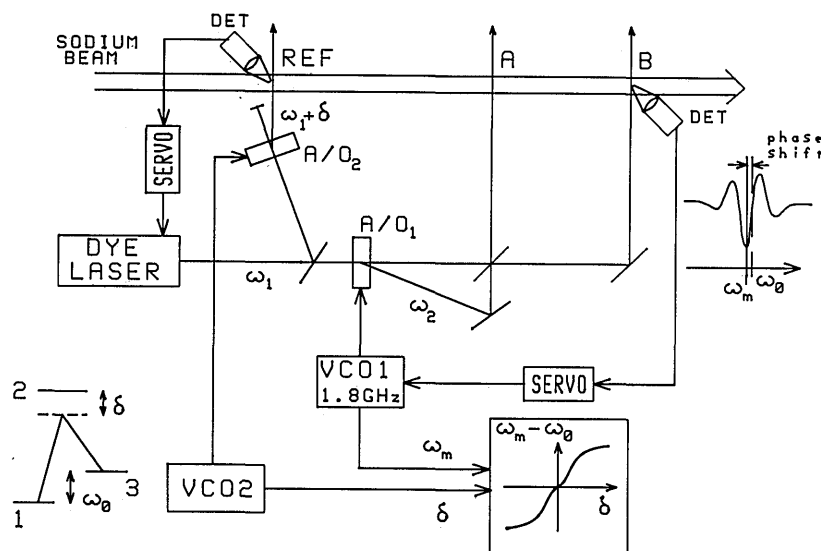


Fig. 4. Schematic of experimental setup for measuring the ac Stark shift as a function of common-mode laser detuning. DET's, detectors.

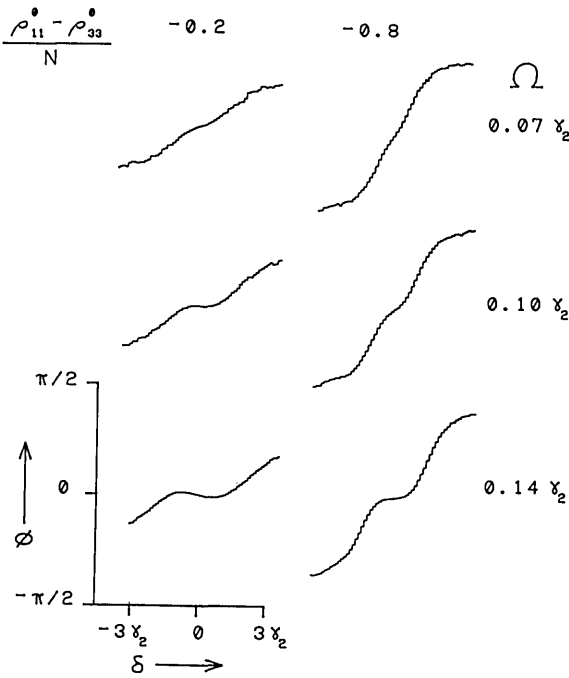


Fig. 5. Data showing the ac Stark shift as a function of common-mode laser detuning, for several combinations of laser intensity and initial populations, as labeled.

as a function of common-mode laser detuning,  $\delta$ , where  $\delta$  varies from  $-3.2\gamma_2$  to  $+3.2\gamma_2$ , a total range of  $\sim 6.4$  times the state 2 linewidth. The values of average<sup>10</sup> laser intensity (at zones A and B) and the initial atomic state population differences are as indicated. To simplify comparison with theory, the observed ac Stark shifts are expressed in units of Ramsey-fringe phase shift, where a  $\pi/2$  phase shift corresponds to

a frequency shift of the central fringe minimum by one fourth of the 2.3-kHz fringe spacing.

Examination of the data in Fig. 5 shows that, at low laser intensities (top row), the ac Stark shift is nearly linear with laser detuning, for detunings less than  $2\gamma_2$ . The slope is determined by the initial state 1 and 3 populations, where larger population differences produce larger ac Stark shifts. In contrast, for higher laser intensities in zones A and B (middle and bottom rows), the ac Stark shift is smaller, near zero laser detuning. However, for larger laser detunings (greater than  $\sim 2\gamma_2$ ), the ac Stark shift is once again determined primarily by initial state 1 and 3 populations, as in the low-intensity data. In all cases, the ac Stark shift never exceeds  $\pi/2$ .

### THEORY

To calculate the Ramsey-fringe line shape (and ac Stark shifts) that are observed in the zone B fluorescence, the time-dependent density-matrix equations are the natural choice. These density-matrix equations have been derived

by many authors,<sup>2</sup> and the procedure will only be reviewed here. The relevant density-matrix equations are as follows:

$$\dot{\rho}_{11} = -(\frac{1}{2}i\Omega_1\alpha_{12} + \text{c.c.}) + \Gamma_{21}\rho_{22}, \quad (1a)$$

$$\dot{\rho}_{22} = (\frac{1}{2}i\Omega_1\alpha_{12} + \text{c.c.}) + (\frac{1}{2}i\Omega_2\alpha_{32} + \text{c.c.}) - \gamma_2\rho_{22}, \quad (1b)$$

$$\dot{\rho}_{33} = -(\frac{1}{2}i\Omega_2\alpha_{32} + \text{c.c.}) + \Gamma_{23}\rho_{22}, \quad (1c)$$

$$\dot{\alpha}_{12} = \frac{1}{2}i\Omega_1^*(\rho_{22} - \rho_{11}) - \frac{1}{2}i\Omega_2^*\alpha_{13} - (\frac{1}{2}\gamma_2 + i\delta_1)\alpha_{12}, \quad (1d)$$

$$\dot{\alpha}_{32} = \frac{1}{2}i\Omega_2^*(\rho_{22} - \rho_{33}) - \frac{1}{2}i\Omega_1^*\alpha_{13}^* - (\frac{1}{2}\gamma_2 + i\delta_2)\alpha_{32}, \quad (1e)$$

$$\dot{\alpha}_{13} = \frac{1}{2}i\Omega_1^*\alpha_{32}^* - \frac{1}{2}i\Omega_2\alpha_{12} - i(\delta_1 - \delta_2)\alpha_{13}, \quad (1f)$$

In these equations, the usual rotating-wave, electric-dipole, and semiclassical field approximations are employed. The electric field is assumed to have the following form:

$$\mathbf{E}(\mathbf{r}, t) = \frac{1}{2}(\mathbf{E}_1(\mathbf{r})\exp(-i\omega_1 t) + \text{c.c.}) + \frac{1}{2}(\mathbf{E}_2(\mathbf{r})\exp(-i\omega_2 t) + \text{c.c.}) \quad (2)$$

All remaining notations are defined in Table 1.

By making the three additional approximations listed in Table 2, the density-matrix equations can be reduced to the following simple form:

$$\frac{d}{dt} \begin{bmatrix} 2 \text{Re } \alpha_{13} \\ 2 \text{Im } \alpha_{13} \\ \rho_{11} - \rho_{33} \end{bmatrix} = A \begin{bmatrix} 2 \text{Re } \alpha_{13} \\ 2 \text{Im } \alpha_{13} \\ \rho_{11} - \rho_{33} \end{bmatrix} + B, \quad (3a)$$

where the observable fluorescence can be obtained from the following:

$$\rho_{22} = \frac{\Omega^2 S f}{\gamma_2} [N + d(\rho_{11} - \rho_{33}) + g(2 \text{Re } \alpha_{13})]. \quad (3b)$$

Here,

$$A = \begin{bmatrix} -[1 - g^2(1 - f)]\Omega^2 S & (\Delta - d\Omega^2 D) & gd(1 - f)\Omega^2 S \\ -(\Delta - d\Omega^2 D) & -\Omega^2 S & -g\Omega^2 D \\ [rdf + gd(1 - f)]\Omega^2 S & g\Omega^2 D & [rdf - 1 + d^2(1 - f)]\Omega^2 S \end{bmatrix}, \quad (3c)$$

$$B = N\Omega^2 S \begin{bmatrix} -gf \\ 0 \\ (r - d)f \end{bmatrix}. \quad (3d)$$

$N$  is the total number of atoms in the system, and the remaining quantities are defined in Table 3. These equations represent the complete solution of the Raman process in the interaction zones, within the listed approximations.

In the dark zone, the density-matrix equations simplify to

$$\frac{d}{dt} \begin{bmatrix} 2 \text{Re } \alpha_{13} \\ 2 \text{Im } \alpha_{13} \\ \rho_{11} - \rho_{33} \end{bmatrix} = \begin{bmatrix} 0 & \Delta & 0 \\ -\Delta & 0 & 0 \\ 0 & 0 & 0 \end{bmatrix} \begin{bmatrix} 2 \text{Re } \alpha_{13} \\ 2 \text{Im } \alpha_{13} \\ \rho_{11} - \rho_{33} \end{bmatrix} \quad (4a)$$

and

$$\rho_{22} = 0. \quad (4b)$$

Clearly, to compute the Ramsey-fringe line shapes one must combine these two solutions. To illustrate this, the approximations listed in Table 4 will be employed in order to simplify the problem. With these approximations, the den-

**Table 1. Definitions Used in Eq. (1)**

Description	Defining Equation
Laser detuning of $\omega_1$	$\delta_1 = \omega_1 - (\epsilon_2 - \epsilon_1)/\hbar$
Laser detuning of $\omega_2$	$\delta_2 = \omega_2 - (\epsilon_2 - \epsilon_3)/\hbar$
Unperturbed energy levels	$\epsilon_1, \epsilon_2, \epsilon_3$
Rabi frequency for 1-2 transition	$\Omega_1 = (\mu_{21} \cdot \mathbf{E}_1)/\hbar$
Rabi frequency for 3-2 transition	$\Omega_2 = (\mu_{23} \cdot \mathbf{E}_2)/\hbar$
Rotating-wave density-matrix elements	$\begin{cases} \alpha_{12} = \rho_{12} \exp(-i\omega_1 t) \\ \alpha_{32} = \rho_{32} \exp(-i\omega_2 t) \\ \alpha_{13} = \rho_{13} \exp(-i(\omega_1 - \omega_2)t) \end{cases}$
Within-system decay rates	$\Gamma_{21}, \Gamma_{23}$
Total state 2 decay rate	$\gamma_2$

**Table 2. Approximations Used in Eq. (3)**

Description	Mathematical Form
State 2 short-lived compared with single-zone transit-time partial steady state	$\begin{cases} \rho_{22} \ll \gamma_2 \rho_{22} \\ \dot{\alpha}_{12} \ll (\frac{1}{2}\gamma_2 + i\delta_1)\alpha_{12} \\ \dot{\alpha}_{32} \ll (\frac{1}{2}\gamma_2 + i\delta_2)\alpha_{32} \end{cases}$
Small laser difference frequency detuning (compared with correlated laser detuning or state 2 decay rate)	$\delta_1 - \delta_2 \ll \delta_1, \delta_2, \gamma_2$
Closed system	$\Gamma_{21} + \Gamma_{23} = \gamma_2$

**Table 3. Definitions Used in Eq. (3)**

Description	Defining Equation
Common-mode laser detuning	$\delta = \frac{1}{2}(\delta_1 + \delta_2)$
Laser difference frequency detuning	$\Delta = (\delta_1 - \delta_2)$
Average (squared) Rabi frequency	$\Omega^2 = \frac{1}{2}( \Omega_1 ^2 +  \Omega_2 ^2)$
Raman damping rate	$\Omega^2 S = \Omega^2 \frac{\gamma_2}{\gamma_2^2 + 4\delta^2}$
Raman dispersion	$\Omega^2 D = \Omega^2 \frac{\delta}{\gamma_2^2 + 4\delta^2}$
Normalized difference of (squared) Rabi frequencies	$d = \frac{ \Omega_1 ^2 -  \Omega_2 ^2}{ \Omega_1 ^2 +  \Omega_2 ^2}$
Normalized product of Rabi frequencies	$g = 2 \frac{ \Omega_1 \Omega_2^* }{ \Omega_1 ^2 +  \Omega_2 ^2}$
Raman saturation parameter	$f = \frac{\gamma_2}{\gamma_2 + 3\Omega^2 S}$
Normalized difference of within-system decay rates	$r = \frac{\Gamma_{21} - \Gamma_{23}}{\gamma_2}$

**Table 4. Approximations Used in Eq. (5)**

Description	Defining Equation
Equal Rabi frequency	$d = 0, g = 1$
Equal within-system decay rates	$r = 0$
Small laser difference frequency detuning (compared with single-zone linewidth)	$\Delta \ll \Omega^2 S$

sity-matrix equations in the interaction zones reduce to the following:

$$\frac{d}{dt} \begin{bmatrix} 2 \operatorname{Re} \alpha_{13} \\ 2 \operatorname{Im} \alpha_{13} \\ \rho_{11} - \rho_{33} \end{bmatrix} = \begin{bmatrix} f\Omega^2 S & 0 & 0 \\ 0 & -\Omega^2 S - \Omega^2 D & 0 \\ 0 & \Omega^2 D & -\Omega^2 S \end{bmatrix} \begin{bmatrix} 2 \operatorname{Re} \alpha_{13} \\ 2 \operatorname{Im} \alpha_{13} \\ \rho_{11} - \rho_{33} \end{bmatrix} + N \begin{bmatrix} -f\Omega^2 S \\ 0 \\ 0 \end{bmatrix} \quad (5a)$$

and

$$\rho_{22} = \frac{\Omega^2 S f}{\gamma_2} (N + 2 \operatorname{Re} \alpha_{13}). \quad (5b)$$

The initial conditions for solving these equations are simple at zone A:  $\alpha_0^{13} = 0$ , and  $(\rho_{11}^0 - \rho_{33}^0)$  is determined by optical pumping in the reference zone. For the dark zone and zone B, the initial conditions are of course obtained from the solution to the previous zone. Performing this calculation, for a rectangular laser beam profile, leads to the following expression<sup>11</sup> for the observable (spatially integrated) fluorescence in zone B:

$$\int_T^{T+T_B} \gamma_2 \rho_{22} dt = N [1 - \exp(-f\Omega^2 S_B \tau_B)] \times \{1 + [1 - \exp(-f\Omega^2 S_A \tau_A)] |\sec \phi| \cos(\Delta T - \phi)\}, \quad (6a)$$

where  $\phi$  is the phase of the complex Raman-Ramsey fringes and is given by

$$\begin{aligned} \tan \phi &= \frac{\operatorname{Im} \alpha_{13}(\tau_A)}{\operatorname{Re} \alpha_{13}(\tau_A)} \\ &= - \frac{(\rho_{11}^0 - \rho_{33}^0) \sin(\Omega^2 D_A \tau_A) \exp(-\Omega^2 S_A \tau_A)}{N [1 - \exp(-f\Omega^2 S_A \tau_A)]}. \end{aligned} \quad (6b)$$

Here  $\tau_A$  and  $T_s$  are the transit times in zones A and B, respectively, and  $T$  ( $\gg \tau_A, \tau_B$ ) is the dark-zone transit time. Note that the phase shift depends totally on zone A (no zone B contribution) and in fact is equal to the phase of the (complex) Raman polarization,  $\alpha_{13}(\tau_A)$ , at the end of zone A. Other features of this expression will be illustrated below.

When unequal laser intensities are included, the expression for the Ramsey-fringe phase become

$$\tan \phi = - \frac{(\rho_{11}^0 - \rho_{33}^0) \sin(\Omega^2 D \tau) \exp(-\Omega^2 S \tau)}{N [1 - \exp(-f\Omega^2 S \tau)] + \xi d}, \quad (7a)$$

where

$$\xi = (\rho_{11}^0 - \rho_{33}^0) \{\cos(\Omega^2 D \tau) - \exp[(1-f)\Omega^2 S \tau]\} \exp(-\Omega^2 S \tau) \quad (7b)$$

and the zone A subscripts have been dropped for simplicity. This expression shows that the ac Stark shift for unequal Rabi frequencies ( $d \neq 0$ , where  $d$  is defined in Table 3) is nearly identical to the equal Rabi frequency case, except for an additional term,  $d\xi$ , in the denominator. Under the conditions of our experiment this additional term is small. Thus the two-zone ac Stark shift is not highly sensitive to

differences in laser intensities as long as the sum of the two Rabi frequencies (or laser intensities) remains unchanged.

**COMPARISON OF THEORY AND EXPERIMENT**

Figure 6 shows six theoretical plots of the two-zone ac Stark shift [Eq. 6(b)] versus laser detuning. Each plot was generated by using values of laser intensities and initial atomic state populations obtained from the experimental conditions of the corresponding data in Fig. 5. No free parameters were used. As can be seen, these theoretical plots agree qualitatively with the experimental results, even though the theory assumes rectangular laser intensity profiles<sup>10,11</sup> and single-velocity atoms.<sup>12,13</sup> In particular, the calculations successfully predict the suppression of the two-zone ac Stark shift for increasing laser intensities (near zero detuning) as well as the general increase in ac Stark shifts with increasing initial population differences. The only discrepancy is the failure of the theory to predict correctly the reversal of slope seen in the lower left-hand experimental trace of Fig. 5. It will be shown below how this can be explained by using the fact that sodium is not a three-level system.

To test the predicted insensitivity of the ac Stark shift to differences in Rabi frequencies (or intensities) of the two laser fields, additional data were obtained for unequal Rabi frequencies. These data are shown in the top trace of Fig. 7 for the case when the laser field at  $\omega_1$  has twice the intensity ( $\sqrt{2}$  times the Rabi frequency) of the laser field at  $\omega_2$  ( $d = 1/3$ , where  $d$  is defined in Table 3). For these data the average intensity is  $\Omega = 0.12\gamma_2$ , and the initial atomic state population difference is  $\rho_{11}^0 - \rho_{33}^0 = 0.8$ . These values are similar to those of the bottom right-hand trace in Fig. 5. A theoretical plot corresponding to these data appears as the middle trace in Fig. 7. As in the equal-Rabi-frequency case, the agreement between theory and experiment is good. The

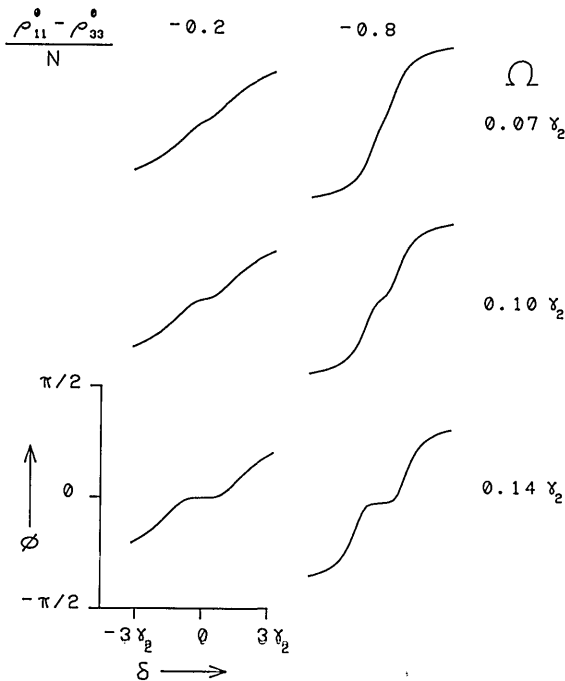


Fig. 6. Calculated ac Stark shift, for conditions corresponding to the data presented in Fig. 5.

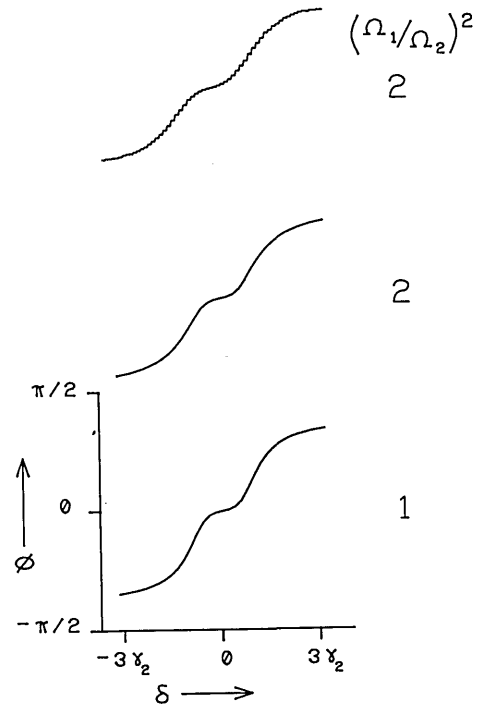


Fig. 7. Illustration of the insensitivity of the ac Stark shift to differences in Rabi frequencies. (Top trace) Data showing the ac Stark shift for unequal Rabi frequencies,  $|\Omega_1/\Omega_2| = \sqrt{2}$ . (Middle trace) Theoretical ac Stark shift for  $|\Omega_1/\Omega_2| = \sqrt{2}$ . (Bottom trace) Theoretical ac Stark shift for  $|\Omega_1| = |\Omega_2|$  but same  $(|\Omega_1|^2 + |\Omega_2|^2)$ .

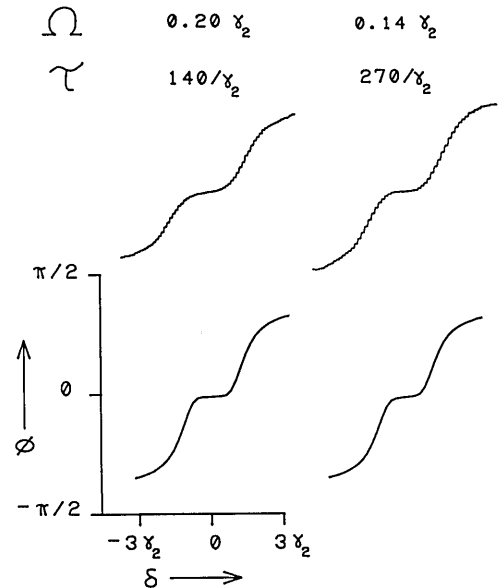


Fig. 8. Illustration of insensitivity of the ac Stark shift to the exact laser beam profile. Zone A transit times,  $\tau$ , are as indicated ( $\Omega^2\tau$  remains constant). Top traces are experimental, bottom traces are theory.

bottom trace is included for comparison and was calculated by using the equal-Rabi-frequency expression [Eq. (6b)] for the same average Rabi frequency,  $\Omega^2 = \frac{1}{2}(|\Omega_1|^2 + |\Omega_2|^2)$ . Clearly, in this case the ac Stark shift is nearly insensitive to the differences in the Rabi frequencies for the 1=2 and 3=2 transitions.

To test the effects of different laser beam profiles on the two-zone ac Stark shift, Fig. 8 shows data obtained for two

different laser beam sizes (in both zones A and B), where the intensities are adjusted such that the time-integrated intensity as seen by the moving atom ( $\Omega^2\tau$  for rectangular profile) is the same. In a two-level system, this would be analogous to using, for example, two  $\pi$  pulses ( $\Omega\tau = \pi$ ) of different shape. The upper right-hand trace in Fig. 8 corresponds to a large laser beam and in fact is a reproduction of the lower right-hand trace in Fig. 5. Next, the laser power is reduced by approximately half, and the laser beams are focused to approximately half of the original diameters in both zones A and B. Data obtained under these conditions are shown in the upper left-hand trace of Fig. 8. As can be seen, the two upper traces of Fig. 8 are nearly identical, verifying that the exact laser beam profile is relatively unimportant, as long as the time-integrated intensity as seen by the moving atom remains unchanged.<sup>11</sup> The bottom two traces in Fig. 8 show the corresponding theoretical plots, obtained from Eq. (6b). Again, theory and experiment show qualitative agreement.

### THEORY INCLUDING ZEEMAN SUBLEVELS OF SODIUM

As mentioned above, agreement between experiment and theory was generally good except for the case (lower-left-hand trace of Fig. 5) in which a slope reversal near zero detuning was seen experimentally but not predicted theoretically. To explain this, it is necessary to consider the fact that sodium is not a perfect three-level system but has many Zeeman sublevels. Figure 9 shows the Zeeman sublevels of the sodium hyperfine states involved in the Raman interaction in our experiment. The allowed Raman transitions between these Zeeman levels (for right-circularly polarized laser light, as used in the experiment) are shown as solid lines. As mentioned above, a small ( $\sim 60$ -mG) magnetic field, directed parallel to the laser  $\mathbf{k}$  vectors, is used to lift the Zeeman degeneracy. The two heavy solid lines show the  $m = 0, \Delta m = 0$  Raman transition that was used for our two-zone studies. The dotted lines show the additional transitions allowed for fluorescent decay. Relative matrix elements (squared) are shown near the bottom levels.

As can be seen from Fig. 9, state 2 decays to levels other than states 1 and 3, just as states 1 and 3 see an influx of atoms from upper Zeeman sublevels other than state 2. Because of these additional decay paths, the influx of populations to states 1 and 3 is not determined entirely by the within-system decay rates from state 2, as was the case for a closed three-level system. We are currently investigating the complex dynamics of the sodium system, using numerical methods. However, it should be possible to include the effects of the additional Zeeman levels to first order by introducing effective, unequal within-system decay rates,  $\Gamma_{21} \neq \Gamma_{23}$  (or  $r \neq 0$ ), to the closed three-level system equations. When this is done, the Ramsey-fringe phase is given by

$$\tan \phi = -\frac{(\rho_{11}^0 - \rho_{33}^0)[\sin(\Omega^2 D\tau)]\exp(-\Omega^2 S\tau) + r\zeta}{N\{1 - \exp[-(f - rdf)\Omega^2 S\tau]\} + d\xi' - r\eta}, \quad (8a)$$

where

$$\zeta = \frac{1}{2}\Omega^2 S[EH - FG][N + d(\rho_{11}^0 - \rho_{33}^0)], \quad (8b)$$

$$\eta = \frac{1}{2}df\Omega^2 S[EG + FH][N - d(\rho_{11}^0 - \rho_{33}^0)], \quad (8c)$$

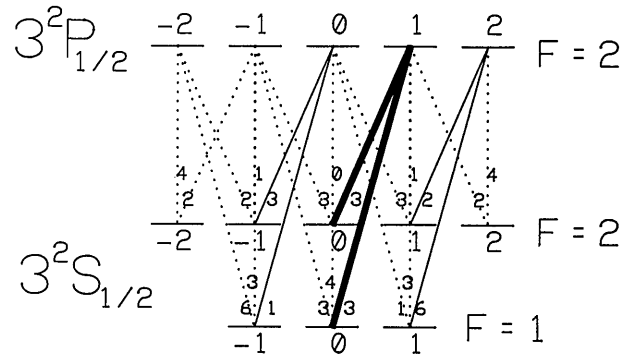


Fig. 9. Sodium hyperfine states involved in Raman interaction, for circularly polarized light. Solid lines are possible Raman transitions. Heavy solid lines show the  $m = 0, \Delta m = 0$  Raman transitions used in these two-zone studies. Dotted lines are spontaneous decay paths. Number are relative matrix elements squared.

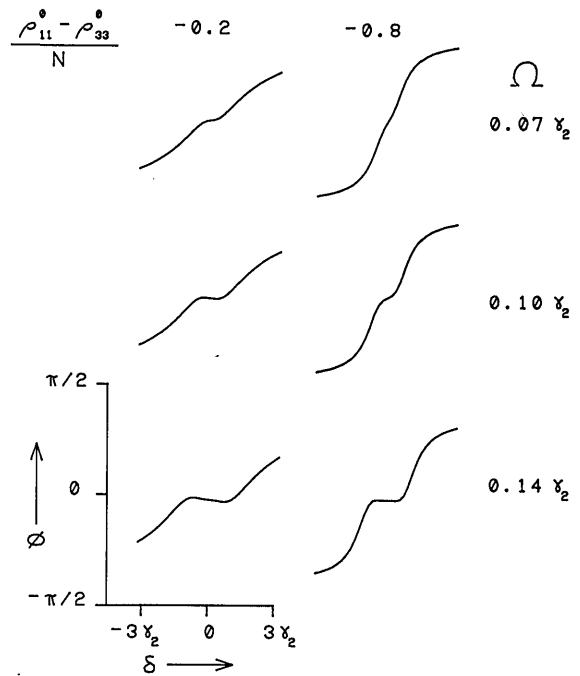


Fig. 10. Revised theoretical plots of the ac Stark shift, for conditions corresponding to the data presented in Fig. 5. Effects of nearby magnetic sublevels are included to first order by using an effective normalized difference of within-system decay rates,  $r' = 0.275$ .

$$\xi' = (\rho_{11}^0 - \rho_{33}^0)E, \quad (8d)$$

$$E = \{\cos(\Omega^2 D\tau) - \exp[(1 - f + rdf)\Omega^2 S\tau]\}\exp(-\Omega^2 S\tau), \quad (8e)$$

$$F = [\sin(\Omega^2 D\tau)]\exp(-\Omega^2 S\tau), \quad (8f)$$

$$G = \frac{2\Omega^2 S(1 - f + rdf)}{[\Omega^2 S(1 - f + rdf)]^2 + [\Omega^2 D]^2}, \quad (8g)$$

$$H = \frac{-2\Omega^2 D}{[\Omega^2 S(1 - f + rdf)]^2 + [\Omega^2 D]^2}, \quad (8h)$$

and, as before, the phase shift is determined entirely by the zone A interaction.

To estimate an effective value of  $r$  (denoted by  $r'$ ), it is first necessary to compute the total rate of population influx to states 1 and 3 from all levels. These rates will be called  $\Gamma_{21}'$

and  $\Gamma_{23}'$ , respectively. The effective value of  $r$  is then simply  $r' = (\Gamma_{21}' - \Gamma_{23}')/(\Gamma_{21}' + \Gamma_{23}')$ . To illustrate this, values of  $r'$  will now be computed for two cases. First, assuming nearly equal initial populations in all the Zeeman ground-state sublevels, we compute an effective value of  $r' = 0.22$ , neglecting any optical pumping. Second, it is assumed that the  $F = 1$  hyperfine ground sublevels are initially unpopulated but that the Zeeman sublevels in the  $F = 2$  ground state are equally populated. Such an initial population distribution might be produced, for example, by a strong reference beam. In this case  $r' = 0.33$ . Averaging this and the previous value of  $r'$  gives  $r' = 0.275$ .

Using this effective value of  $r$  in Eqs. (8) results in the theoretical plots of Fig. 10, where as before the laser intensities and initial atomic state populations are obtained from the corresponding data in Fig. 5. As can be seen, the lower left-hand plot in Fig. 10 now shows much better agreement with the data. In particular, the slope reversal of the ac-Stark shift versus laser detuning is now correctly predicted.<sup>14</sup>

### SUPPRESSION OF ac STARK SHIFTS

Theoretically, inspection of Eqs. (6b) and (7a) predicts that the two-zone ac Stark shift should be exactly zero if the initial population difference between states 1 and 3 is zero. In the present sodium experiment this is not observed because optical pumping between Zeeman levels in the interaction zones always redistributes the populations somewhat. If a closed three-level system cannot be found, theory predicts that the ac Stark shift can still be reduced to arbitrarily small levels by strongly saturating the zone A interaction (i.e., high laser intensities or long interaction times).

In the present setup, however, we are limited in our choice of atomic systems and in our maximum laser intensities and interaction times. Nonetheless, the observed reversal of slope in the ac Stark shift near zero laser detuning suggests that for a range of (fixed) laser intensities, the initial atomic state populations can be adjusted so as to reduce the ac Stark shift greatly, even within the limitations of the present setup.

To this end, Fig. 11(a) shows a high-resolution experimental plot of the ac Stark shift versus laser detuning obtained

under the following experimental conditions, chosen so as to minimize the ac Stark shift near zero laser detuning:  $\Omega = 0.13\gamma_2$ ,  $(\rho_{11}^0 - \rho_{33}^0) = 0.7N$ . These data are shot-noise limited, obtained with an averaging time of 1 sec.

As can be seen from Fig. 11(a), the ac Stark shift is less than the noise over a laser detuning of nearly  $\pm 0.2\gamma_2$ . For comparison, Fig. 11(b) shows the theoretical ac Stark shift under these experimental conditions, where  $r'$  is used as a free parameter to produce the flattest trace. Clearly, good agreement between theory and experiment is achieved, where the fitted value of  $r'$  is 0.270, which is close to the approximated value of 0.275. Of course, a complete numerical treatment of the sodium system would not require the use of any free parameters. Nonetheless, Fig. 11 shows that even a simple first-order correction to the closed three-level system results is sufficient to give good agreement with data under the conditions of our experiment.

The data of Fig. 11(a) demonstrate an ac Stark shift of less than 0.0014 rad over a laser detuning of nearly  $\pm 0.2\gamma_2$ . For clock applications, this corresponds to a projected stability of better than  $2 \times 10^{-11}$  for a laser detuning of  $0.01\gamma_2$  (100 kHz for sodium). Here it should be noted that this result is still preliminary and does not represent the ultimate achievable clock performance. Nonetheless, these data demonstrate that, by proper choice of experimental conditions, the ac Stark shift can be greatly reduced, even within the limitations of the present experimental setup.

### SUMMARY AND FUTURE WORK

We have measured the ac Stark effect in a two-zone stimulated Raman interaction in a sodium atomic beam. In addition, we have derived simple theoretical expressions for the ac Stark shift, based on a closed three-level system, in the  $\Lambda$  configuration and have achieved qualitative agreement with the data. In particular, the magnitude and sense of the ac Stark shifts are found to depend on laser intensities as well as on the initial populations of the two low-lying levels of the  $\Lambda$  configuration. Specifically, the ac Stark shifts are smaller for larger laser intensities and also for smaller initial population differences between the two low-lying levels. Moreover, the ac Stark shift is shown to be insensitive to the ratio of the intensities of the two laser frequencies, provided that the sum of the two intensities is fixed. The ac Stark shift is also shown to be insensitive to changes in laser-beam profiles as long as the time-integrated intensity as seen by the moving atom remains unchanged. Quantitative agreement between ideal three-level theory and experiment is improved when the effects of the numerous Zeeman sublevels in sodium are taken into account to first order. Finally, the experimentally observed reversal of ac Stark shift was used in identifying conditions under which the ac Stark shift can be reduced to levels low enough to be acceptable for potential clock applications.

Future plans are to verify that the ac Stark shift can be further suppressed by increasing the degree of Raman saturation (i.e., large  $\Omega^2 S\tau$ ). This can be achieved either by increasing the laser intensity or by slowing down the atoms (by cooling, for example). In addition, numerical calculations are in progress to identify the exact role played by the Zeeman sublevels and also to include the effects of velocity averaging.<sup>12</sup>

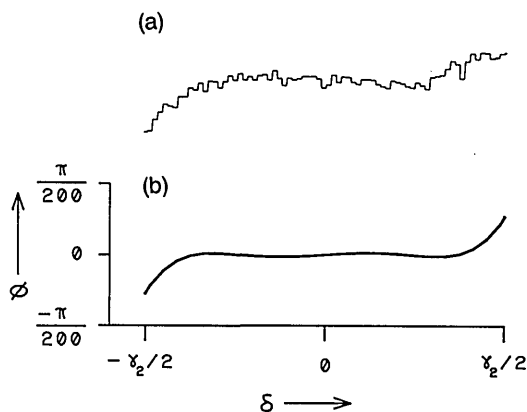


Fig. 11. High-resolution ac Stark shift versus laser detuning: (a) experimental trace for  $\Omega = 0.13\gamma_2$ ,  $(\rho_{11}^0 - \rho_{33}^0) = 0.7N$ , and (b) corresponding theoretical best fit, with  $r' = 0.27$ .

## ACKNOWLEDGMENTS

We thank John Kierstead for his valuable support.

This research was supported by the Rome Air Development Center and the Joint Services Electronics Program.

\* Present address, University of Illinois, Urbana-Champaign, Urbana, Illinois 61801.

## REFERENCES AND NOTES

- For example, B. J. Dalton, T. D. Kieu, and P. L. Knight, "Theory of ultra-high-resolution optical Raman Ramsey spectroscopy," *Opt. Acta* **33**, 459 (1986); D. Pegg, "Interaction of three-level atoms with modulated lasers," *Opt. Acta* **33**, 363 (1986); N. I. Shamrov, "Induced transparency in resonant induced Raman scattering," *Zh. Prikl. Spektrosk.* **40**, 346 (1984); S. Swain, "Conditions for population trapping in a three-level system," *J. Phys. B* **15**, 3405 (1982); P. M. Radmore and P. L. Knight, "Population trapping and dispersion in a three-level system," *J. Phys. B* **15**, 561 (1982); G. Orriols, "Nonabsorption resonances by nonlinear coherent effects in a three-level system," *Nuovo Cimento B* **53**, 1 (1979); H. R. Gray, R. M. Whitley, and C. R. Stroud, Jr., "Coherent trapping of atomic populations," *Opt. Lett.* **3**, 218 (1978); A. Szoke and E. Courtens, "Time-resolved resonance fluorescence and resonance Raman scattering," *Phys. Rev. Lett.* **34**, 1053 (1975).
- P. L. Knight, M. A. Lauder, P. M. Radmore, and B. J. Dalton, "Making atoms transparent: trapped superpositions," *Acta Phys. Austriaca* **56**, 103 (1984); F. H. Mies and Y. B. Aryeh, "Kinetics and spectroscopy of near-resonant optical pumping in intense fields," *J. Chem. Phys.* **74**, 53 (1981); E. Courtens and S. Szoke, "Time and spectral resolution in resonance scattering and resonance fluorescence," *Phys. Rev. A* **15**, 1588 (1977); M. Sargent III and P. Horwitz, "Three-level Rabi flopping," *Phys. Rev. A* **13**, 1962 (1976); R. G. Brewer and E. L. Hahn, "Coherent two-photon processes: transient and steady state cases," *Phys. Rev. A* **11**, 1641 (1975).
- J. Mlynek and R. Grimm, "Raman heterodyne Ramsey spectroscopy in a samarium atomic beam" *Appl. Phys. B* **45**, 77 (1988); M. Kaivola, P. Thorsen, and O. Poulsen, "Dispersive line shapes and optical pumping in a three-level system," *Phys. Rev. A* **32**, 207 (1985); F. Shimizu, K. Shimizu, and H. Takuma, "Selective vibrational pumping of a molecular beam by a stimulated Raman process," *Phys. Rev. A* **31**, 3132 (1985); A. Sharma, W. Happer, and Y. Q. Lu, "Sub-Doppler-broadened magnetic field resonances in the resonant stimulated electronic Raman scattering of multimode laser light," *Phys. Rev. A* **29**, 749 (1984); R. E. Tench and S. Ezekiel, "Precision measurements of hyperfine predissociation in I<sub>2</sub> vapor using a two-photon resonant scattering technique," *Chem. Phys. Lett.* **96**, 253 (1983); R. E. Tench, B. W. Peuse, P. R. Hemmer, J. E. Thomas, S. Ezekiel, C. C. Leiby Jr., R. H. Picard, C. R. Willis, "Two laser Raman difference frequency technique applied to high precision spectroscopy," *J. Phys. Colloq.* **42**, 45 (1981); P. Kumar and J. H. Shapiro, "Observation of Raman-shifted oscillation near the sodium D lines," *Opt. Lett.* **10**, 226 (1985); M. S. Feld, M. M. Burns, T. U. Kuhl, P. G. Pappas, and D. E. Murnick, "Laser-saturation spectroscopy with optical pumping," *Opt. Lett.* **5**, 79 (1980); G. Alzetta, L. Moi, and G. Orriols, "Nonabsorption hyperfine resonances in a sodium vapor irradiated by a multimode dye-laser," *Nuovo Cimento B* **52**, 209 (1979); R. P. Hackel and S. Ezekiel, "Observation of subnatural linewidths by two-step resonant scattering in I<sub>2</sub> vapor," *Phys. Rev. Lett.* **42**, 1736 (1979); K. Takagi, R. F. Curl, and R. T. M. Su, "Spectroscopy with modulation sidebands," *Appl. Phys.* **7**, 181 (1975); R. L. Shoemaker and R. G. Brewer, "Two-photon superradiance," *Phys. Rev. Lett.* **28**, 1430, (1972).
- E. Buhr and J. Mlynek, "Collision-induced Ramsey resonances in Sm vapor," *Phys. Rev. Lett.* **57**, 1300 (1986); A. A. Dabagyan, M. E. Movsesyan, T. O. Ovakimyan, and S. V. Shmavonyan, "Stimulated processes in potassium vapor in the presence of a buffer gas," *Sov. Phys. JETP* **58**, 700 (1983).
- D. Krokkel, K. Ludewigt, and H. Welling, "Frequency up-conversion by stimulated hyper-Raman scattering," *IEEE J. Quantum Electron.* **QE-22**, 489 (1986); R. S. F. Chang, M. T. Duignan, R. H. Lehmberg, and N. Djeu, "Use of stimulated Raman scattering for reducing the divergence of severely aberrated laser beams," in *Excimer Lasers: Their Applications and New Frontiers in Lasers*, R. W. Waynank, ed., Proc. Soc. Photo-Opt. Eng. **476**, 81 (1984); J. C. White, "Up-conversion of excimer lasers via stimulated anti-Stokes Raman scattering," *IEEE J. Quantum Electron.* **QE-20**, 185 (1984); N. V. Znamenskii and V. I. Odintsov, "Infrared stimulated Raman scattering in rubidium vapor with a tunable pump frequency," *Opt. Spectrosc. (USSR)* **54**, 55 (1983); R. Wyatt, N. P. Ernsting, W. G. Wrobel, "Tunable electronic Raman laser at 16 microns," *Appl. Phys. B* **27**, 175 (1982); M. L. Steyn-Ross and D. F. Walls, "Quantum theory of a Raman laser," *Opt. Acta* **28**, 201 (1981).
- P. R. Hemmer, G. P. Ontai, and S. Ezekiel, "Precision studies of stimulated resonance Raman interactions in an atomic beam," *J. Opt. Soc. Am. B* **3**, 219 (1986); P. R. Hemmer, S. Ezekiel, and C. C. Leiby, Jr., "Stabilization of a microwave oscillator using a resonance Raman transition in a sodium beam," *Opt. Lett.* **8**, 440 (1983); P. Knight, "New frequency standards from ultranarrow Raman resonances," *Nature (London)* **297**, 16 (1982); J. E. Thomas, P. R. Hemmer, S. Ezekiel, C. C. Leiby, Jr., R. H. Picard, and C. R. Willis, "Observation of Ramsey fringes using a stimulated resonance Raman transition in a sodium atomic beam," *Phys. Rev. Lett.* **48**, 867 (1982); J. E. Thomas, S. Ezekiel, C. C. Leiby, Jr., R. H. Picard, and C. R. Willis, "Ultrahigh resolution spectroscopy and frequency standards in the microwave and far-infrared region using optical lasers," *Opt. Lett.* **6**, 298 (1981).
- P. R. Hemmer, V. D. Natoli, M. S. Shahriar, B. Bernacki, H. Lamela-Rivera, S. P. Smith, and S. Ezekiel, in *41st Annual Symposium on Frequency Control* (Institute of Electrical and Electronics Engineers, New York, 1987), p. 42.
- E. De Clercq and P. Cerez, "Evaluation of the light shift in a frequency standard based on Raman induced Ramsey resonance," *Opt. Comm.* **45**, 91 (1983); B. J. Dalton and P. L. Knight, "The effects of laser field fluctuations on coherent population trapping," *J. Phys. B* **15**, 3997 (1982).
- N. F. Ramsey, *Molecular Beams* (Oxford U. Press, London, 1963), Chap. 5, Sec. 3.
- Average laser intensity is defined here by the following:
 
$$(\Omega^2)_{\text{average}} = \frac{1}{\tau_{1/2}} \int_{-\infty}^{\infty} \Omega^2(t) dt,$$
 where  $\tau_{1/2}$  is the atom transit time corresponding to the half-intensity positions on the actual laser beam profile and  $\Omega^2 = \frac{1}{2}(|\Omega_1|^2 + |\Omega_2|^2)$ . Here,  $|\Omega_1|^2$  and  $|\Omega_2|^2$  are the laser intensities at  $\omega_1$  and  $\omega_2$ , respectively, in units of Rabi frequency squared.
- For a nonrectangular laser beam profile,  $\Omega$  is a function of time for a moving atom in the atomic beam. In that case, Eqs. (6a) and (6b) are modified by making the following replacements:
 
$$\Omega^2 \tau \rightarrow \int_{-\infty}^{\infty} \Omega^2(t) dt, \quad f \Omega^2 \tau \rightarrow \int_{-\infty}^{\infty} f(t) \Omega^2(t) dt,$$
 where it is assumed that the two interaction regions do not overlap, so that
 
$$\int (\Omega_A^2 + \Omega_B^2) dt = \int \Omega_A^2 dt + \int \Omega_B^2 dt.$$
 For the intensities used in our experiments,  $f$  is nearly a constant (unity) and can be pulled outside the integral.
- Interaction times and transit times are computed by using the thermal velocity  $v = \sqrt{2kT/M}$  characteristic of a sodium beam produced by a 400°C oven.
- In general, velocity averaging is accomplished by simply performing a weighted average over all the velocities present in the atomic beam. However, in the present case the ac Stark shift was measured by locking to a minimum of a velocity averaged

Ramsey-fringe line shape. This ac Stark shift is not the same as the weighted average of the ac Stark shifts for each atomic velocity. Nevertheless, over the limited ranges of common-mode laser detuning where  $\phi$  and  $\Delta T$  are both small (so that  $\phi \cong \sin \phi$  and  $\Delta T \cong \sin \Delta T$ ) for all velocities included in the average, a relatively simple numerical calculation is possible and is found to agree well with the single-velocity results presented here. Therefore it is anticipated that the complete numerical calcula-

- tion of the Raman two-zone ac Stark effect, including velocity averaging in a thermal sodium beam, will probably give results that are qualitatively similar to those presented in this paper.
14. It should be pointed out that the effective value of  $r$  as indicated is merely an estimate of the first-order correction to the closed three-level-system results. The exact solution of the sodium system is more complex than simply using an effective value of  $r$  and is currently in progress.